

# Molecular structure, multipolar charge density study and nonlinear optical properties of 4-methyl-N-[(5-nitrothiophen-2-ylmethylidene)] aniline

N. BOUKABCHA<sup>a</sup>, A. FEDDAG<sup>a</sup>, R. RAHMANI<sup>a</sup>, A. CHOUAIIH<sup>a\*</sup>, F. HAMZAOU<sup>b</sup>

<sup>a</sup>Laboratory of Technology and Solid Properties, Faculty of Sciences and Technology, University of Mostaganem, 27000 Mostaganem, Algeria

<sup>b</sup>LPFM Académie de Montpellier - France

In this work we present a comparative structural study of the 4-methyl-N-[(5-nitrothiophen-2-ylmethylidene)] aniline molecule using X-ray diffraction and theoretical *ab initio* methods. The title compound is considered as a good candidate for non-linear optical applications. The experimental results were obtained from a high-resolution X-ray diffraction study using the multipolar charge density model of Hansen and Coppens (1978) in which the charge density around the atoms are described with their non-spherical parts. Where the theoretical investigations were performed using the Hartree–Fock (HF) Density Functional Theory (DFT) methods at B3LYP level of theory using 6-31G(d,p) basis set. The knowledge of the analytical function of the electron charge density distribution have led easily to the determination of the net atomic charge  $s$ , molecular dipole moment and the electrostatic potential around the studied compound. The optimized geometry of the title compound was found to be coherent with the structure determined by X-ray diffraction. The calculated HOMO and LUMO energies show also the charge transfer within the molecule. The obtained molecular electrostatic potential from the two methods confirm the nature of the electron charge transfer and locate the electropositive and the electronegative parts. The theoretical predicted non-linear optical properties are much greater than ones of urea.

(Received September 16, 2016; accepted April 5, 2018)

**Keywords:** Charge density, Electrostatic potential, *ab initio*, Nonlinear optical properties

## 1. Introduction

The nonlinear optical (NLO) behavior of organic materials interests several researchers, especially due to their high efficiency [1,2]. It has been shown that the knowledge of the three-dimensional structure of these materials is crucial for understanding the related phenomena observed in telecommunications and optoelectronics applications [3]. In this context, compounds derived from thiophene have recently received special attention due to their interesting NLO properties [4-9]. In addition, thiophene derivatives functionalized with the nitro group are versatile building blocks for the synthesis of donor–acceptor substituted  $\pi$ -conjugated systems for several optical applications [10].

In continuation of our research on the development of organic NLO compounds [11-17], this work presents the structural analysis of 4-methyl-N-[(5-nitrothiophen-2-ylmethylidene)] aniline molecule carried out from a high resolution X-ray refinements using the MOPRO package [18]. The obtained results are compared to theoretical *ab initio* calculations done on an optimized molecule. This study provides also the calculation of polarizability and first hyperpolarizability tensor describing the NLO properties using the Gaussian 03 program [19]. These theoretical investigations were performed using conventional *ab initio* methods based on self-consistent

field molecular orbital Hartree-Fock (HF) theory and density functional theory (DFT) with the 6-31G (d, p) basis set.

## 2. Structural investigation

### 2.1. X-Ray Structure

The crystal structure of 4-methyl-N-[(5-nitrothiophen-2-ylmethylidene)] aniline compound, with chemical formula  $C_{12}H_{10}N_2O_2S$ , has already been described in details by M. Cai *and al.* [20] and structures of similar compounds have been already studied by many researchers [21-25]. In this last article the refinement was based on spherical atomic charge distribution and led a reliability refinement parameter of 4%. The crystallographic details are summarized in Table 1. In order to improve the accuracy of the results we have used the same X-ray diffraction data and carried out a new refinement based on a non-spherical atomic charge distribution as described by Coppens and Hansen [26]. This new investigation led to a localization of the hydrogen atoms and the distribution of the electron charge density around the intermolecular hydrogen bonding C–H...O.

Table 1. Crystal data and spherical refinement details

Empirical formula	C <sub>12</sub> H <sub>10</sub> N <sub>2</sub> O <sub>2</sub> S	
Formula weight	246.28	
Crystal size (mm)	0.2 × 0.18 × 0.12	
Temperature (K)	113 (2)	
Crystal system, space group	Monoclinic, P2 <sub>1</sub> /n	
Unit cell dimensions		
a (Å)	4.7606 (4)	
b (Å)	22.415 (2)	
c (Å)	10.7008 (15)	
β (°)	92.566 (13)	
Wavelength (Å)	0.71073	
Volume (Å <sup>3</sup> )	1140.7 (2)	
Z, calculated density (mg/m <sup>3</sup> )	4/1.303	
F(000)	752	
θ range for data collection	5.02 – 27.51	
Limiting indices	−6 ≤ h ≤ 6, −29 ≤ k ≤ 29, −13 ≤ l ≤ 14	
Reflections collected/unique observed with I ≥ 2σ(I)	14437/2325	
Refinement method	full-matrix	least-squares on F <sup>2</sup> data
Parameters	155	
Goodness of fit on F <sup>2</sup>	1.09	
Final R indices		
R <sub>1</sub>	0.040	
wR <sub>2</sub>	0.098	

## 2.2. Geometry optimization

In this work, full geometry optimization has been performed using the GAUSSIAN03 package [19] and the Gauss-View molecular visualization program [27], at the Becke3-parameter hybrid exchange functions and Lee-Young–Parr correlation functional (B3LYP) level [28, 29] and HF theory [30], using the 6-31G(d,p) basis set by the Bery method [31,32]. The optimized structure of C<sub>12</sub>H<sub>10</sub>N<sub>2</sub>O<sub>2</sub>S is illustrated in Fig. 1 and the corresponding main geometrical parameters (bonds lengths, bond angles and torsion angles) are listed in Tables 2, 3 and 4.

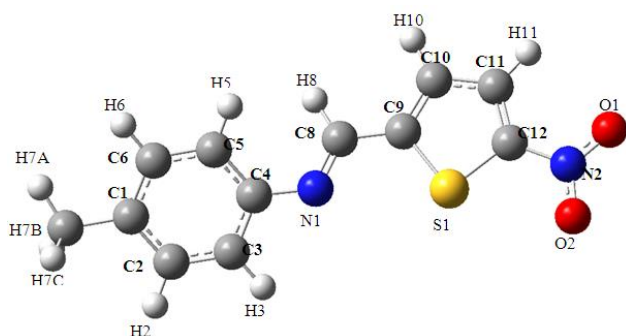


Fig. 1. Optimized structure of the molecule C<sub>12</sub>H<sub>10</sub>N<sub>2</sub>O<sub>2</sub>S.

## 2.3. Electron charge density analysis

### 2.3.1. Multipolar refinement

The Hansen-Coppens multipole formalism, as implemented in the Mopro least-squares program for multipole refinement, was used for the structure factor fitting. This last model describes the crystal electron density as a superposition of non-spherical pseudo-atoms modeled on a multipole expansion given by the following equation:

$$\rho_{atom}(\vec{r}) = \rho_c(\vec{r}) + P_v K'^3 \rho_v(k'\vec{r}) + \sum_l^{l_{max}} \sum_{m=-l}^{+l} K'' R_l(K''\vec{r}) P_{lm} Y_{lm}\left(\frac{\vec{r}}{r}\right) \quad (1)$$

Here  $\rho_c$  and  $\rho_v$  are spherically averaged Hartree-Fock core and valence densities, with  $\rho_v$  being normalized to one electron. The Slater-type radial functions are obtained by:

$$R_l(\vec{r}) = N_l \cdot r_l^{n_j} \exp(-k' \xi_l \vec{r})$$

These functions modulate the spherical harmonic angular functions  $Y_{lm\pm}$  and  $N_l$  is a normalization factor. The values for parameters  $n = n_l$  and  $\xi$  were chosen according to rules provided by Coppens (1997) [33].

The sum over in equation (1) includes  $\pm l$ , so that for each one,  $2l+1$  functions are included. The non-spherical charge density was described at the octapole level ( $l=3$ ) for the atoms C, N and O, the hexadecapole for the S atom ( $l=4$ ) and at the dipole levels ( $l=1$  or  $2$ ) for hydrogen atoms not involved and involved in strong H-bonds, respectively. Charge densities of all hydrogen were considered to have cylindrical symmetry along the corresponding hydrogen-heavy atom bond [34].

During the refinements, the adjustable variables were the valence-shell contraction expansion parameters  $k'$ ,  $k''$ , the population parameter  $P_v$ , and the multipolar parameters  $P_{lm}$  for each atom. In order to reduce the number of these variables, chemical constraints were imposed: atoms with similar environment were assumed to have the same deformation. Also the local symmetry of each atom has been considered.

## 3. Results and discussion

### 3.1. Structural properties

From the results, it can be seen that there is a good agreement between the calculated and the experimental values. The largest deviation between X-ray data and theoretical calculations at the HF/6-31G\*\* level is the N2–O1 distance, around 0.02 Å, and the (C10–C11–C12) angle, which is larger than 1.48°. The B3LYP/6-31G\*\* results deviate in the range from 0.001 to 0.014 Å for bond lengths, and from 0.02° to 1.45° (C7–C1–C6) for bond angles. It can be seen also that there is intramolecular hydrogen bonding between hydrogen atom linked to C8 with oxygen atom O2 in the nitro groups. Some possible

hydrogen bonds are presented in Table 5. Fig. 2 shows the C8–H8...O2 hydrogen bond. These intermolecular interactions stabilize the crystal structure of the title compound.

Table 2. Bond lengths of  $C_{12}H_{10}N_2O_2S$  molecule

Atoms	X-ray	6-31G(d,p)	
		HF	DFT
C1 – C7	1.513(2)	1.525	1.510
C4 – N1	1.431(19)	1.459	1.403
C8 – N1	1.277(2)	1.281	1.283
C8 – C9	1.456(1)	1.466	1.450
C9 – C10	1.374(2)	1.369	1.388
C9 – S1	1.730(15)	1.738	1.744
C10 – C11	1.411(1)	1.422	1.412
C11 – C12	1.364(2)	1.363	1.376
C12 – N2	1.439(19)	1.448	1.435
S1 – C12	1.723(15)	1.733	1.737
N2 – O1	1.227(16)	1.251	1.235
N2 – O2	1.238(16)	1.250	1.237

Table 3. Bond angles of  $C_{12}H_{10}N_2O_2S$  molecule

Atoms	X-ray	6-31G(d,p)	
		HF	DFT
N1 – C4 – C3	117.06(14)	116.64	116.87
C4 – N1 – C8	118.86(13)	124.76	118.96
C6 – C4 – N1	125.10(13)	124.27	125.10
C7 – C1 – C6	121.84(15)	120.69	120.39
C7 – C1 – C2	120.39(15)	121.18	120.39
N1 – C8 – C9	122.04(14)	121.08	122.04
C8 – C9 – C10	125.35(14)	126.88	125.35
C8 – C9 – S1	122.69(11)	120.66	122.70
C9 – C10 – C11	113.49(14)	113.77	113.47
C9 – S1 – C12	89.17(7)	87.75	89.77
C10 – C9 – S1	111.94(12)	112.44	111.94
C10 – C11 – C12	110.57(14)	112.05	110.57
C11 – C12 – N2	125.62(14)	124.92	125.42
S1 – C12 – N2	120.10(11)	121.10	120.11
S1 – C12 – C11	114.25(12)	113.97	114.25
C12 – N2 – O1	118.08(13)	117.93	118.09
C12 – N2 – O2	117.65(13)	117.96	117.55
O1 – N2 – O2	124.27(13)	124.10	124.37

Table 4. Torsion angles of  $C_{12}H_{10}N_2O_2S$  molecule

Atoms	X-ray	6-31G(d,p)	
		HF	DFT
C2 – C3 – C4 – N1	-179.45(13)	-179.49	-179.01
C3 – C4 – N1 – C8	167.13(14)	155.72	145.86
C4 – N1 – C8 – C9	179.73(13)	179.00	179.67
C5 – C4 – N1 – C8	-14.30(2)	-25.67	-36.78
C6 – C5 – C4 – N1	-179.80(14)	-179.87	-179.41
C7 – C1 – C2 – C3	-178.92(14)	-179.41	-179.46
C7 – C1 – C6 – C5	179.55(14)	-179.94	-179.86
N1 – C8 – C9 – C10	-175.90(15)	-179.60	-179.46
N1 – C8 – C9 – S1	5.10(2)	0.36	0.49
C8 – C9 – C10 – C11	-179.16(14)	-179.91	-179.97
C8 – C9 – S1 – C12	179.15(13)	179.99	179.97
C9 – C10 – C11 – C12	0.09(19)	0.02	0.03
C9 – S1 – C12 – C11	0.01(12)	0.05	0.03
C9 – S1 – C12 – N2	-178.17(12)	-179.91	-179.97
C10 – C9 – S1 – C12	0.04(12)	0.06	0.03
C10 – C1 – C12 – S1	-0.06(17)	-0.03	-0.03
C10 – C11 – C12 – N2	178.01(13)	179.93	197.79
C11 – C12 – N2 – O1	2.70(2)	0.17	0.06
C11 – C12 – N2 – O2	-179.72(14)	-179.83	-179.97
C11 – C12 – S1 – C9	0.01(12)	0.03	0.03
S1 – C12 – N2 – O1	-179.35(11)	-179.86	-179.97
S1 – C12 – N2 – O2	1.25(18)	0.13	0.05

Table 5. Hydrogen bonds in  $C_{12}H_{10}N_2O_2S$  crystal by X-ray diffraction

D – H...A	D – H (Å)	D – A (Å)	H – A (Å)	D – H...A (°)
C11–H11...O15	0.930	2.813	2.658	89.80
C5–H5...O2 (1)	0.930	3.417	2.866	119.13
C6–H6...O2 (1)	0.930	3.438	2.900	118.21
C8–H8...O2 (2)	0.930	3.403	2.628	141.24
C10–H10...O2 (2)	0.930	3.533	2.853	130.96
C10–H10...N1(3)	0.930	3.367	2.759	123.84
C3–H3...O1 (4)	0.930	3.584	2.960	125.75
C7–H7A...O1 (5)	0.960	3.386	2.953	108.73
C7–H7A...O2 (6)	0.960	3.305	2.938	104.03
Equivalent positions				
(1) x+1/2, -y+1/2, z-1/2	(2) x+1/2, -y+1/2, z-1/2	(3) x-1/2, -y+1/2, z-1/2		
(4) x+1/2, -y+1/2, z+1/2	(5) -x+1/2, y+1/2, -z+1/2	(6) -x+1/2, y+1/2, -z+1/2		

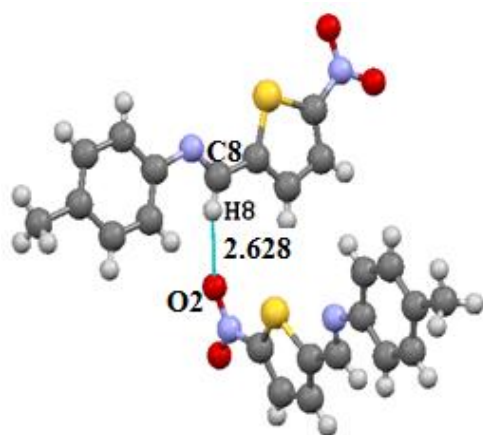


Fig. 2. C8–H8...O2 Hydrogen bond

### 3.2. Electron density maps

The experimental density deformation maps are shown in Figure 3, from which we can observe the

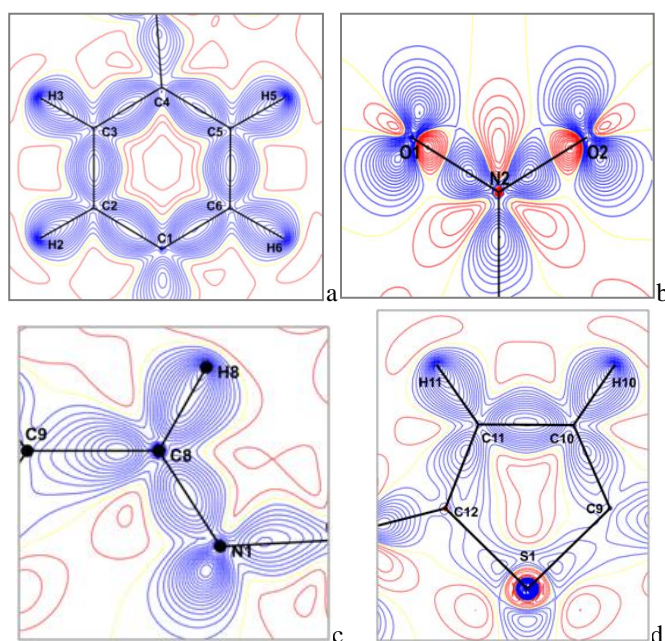


Fig. 3. Electron density maps of  $C_{12}H_{10}N_2O_2S$  molecule in different planes, (a) Benzene ring, (b) Nitro group, (c) C8 = N1 double bond, (d) Thiophene cycle.

We have explored four planes to visualize the electron density distribution; the plane of the aromatic cycle containing the C1, C2, C3, C4, C5 and C6 atoms; the plane containing the electro-acceptor group (Nitro group), the plane formed by the double bond (C8 = N1) and the plane of the thiophene cycle containing the C9, C10, C11, C12 and S1 atoms. Fig. 3 (a, b, c, and d) gives the different maps cited above; all contour intervals are  $0.05 \text{ e} \cdot \text{Å}^{-3}$ .

The almost centered electron density distribution is observed in the middle of the chemical bonds. We also notice that the peaks (Fig. 3 (b)) of the electron density in the connection N2–O1 and N2–O2 are centered towards

absence of the density on the atomic sites and the appearance of all the bond density peaks. The effectiveness of the formalism used for the treatment of data and their quality as proposed by Blessing [35] are confirmed by the obtained maps. This visualization is obtained using the calculated multipolar phases with the observed structure factors  $F_{\text{obs}}(h)$ :

$$\delta\rho^{\text{exp}}(r) = \frac{1}{V} \sum_h [ |F_{\text{obs}}(h)| e^{-i\theta_{\text{mul}}} - |F_{\text{sph}}(h)| e^{-i\theta_{\text{sph}}} ] e^{-2\pi i h r}$$

where  $F_{\text{sph}}(h)$  is computed with atomic positions and thermal parameters. The experimental density map from high-order refinement is  $\rho_{\text{exp}} = \rho_0 - \rho_{\text{sph}}$ , where  $\rho_0$  is the observed electron density and  $\rho_{\text{sph}}$  is the calculated electron density using the atomic parameters obtained from the high-order refinement.

the nitrogen N2 backing the electro donor character of the Nitro group.

These maps allowed us to illustrate the distribution of electronic charges of atoms and chemical bonds along the molecule. We noticed that the lone pairs of oxygen atoms are well resolved. The electron density at sulfur atom is deformed; this deformation can be explained by the effect of a thermal agitation.

The residual map using a non-spherical atom model is shown in Fig. 4, from which we can notice the absence of the density on both the atomic sites and all the bonds. This map confirms the high quality of the data.

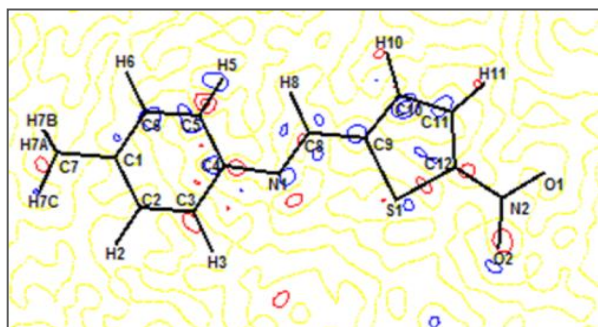


Fig. 4. Residual density map of the  $C_{12}H_{10}N_2O_2S$  molecule, contour  $0.05 \text{ \AA}^{-3}$

### 3.3. Atomic Charges

The valence population coefficients  $P_V^i$  were used to estimate the partial charges on the different atoms according to the following equation:

$$q_i = n_i - P_V^i$$

where  $n_i$  is the total number of electrons of atoms  $i$ . The experimental and theoretical atomic charges are presented in Table 6 and their distribution is shown in Figure 5. The experimental atomic charges derived from the X-ray experiment are generally of the same sign compared to the theoretical ones except some atoms. The expected values are in concordance to the chemical knowledge: H atoms are positively charged, whereas O, S, and N atoms are negatively charged.

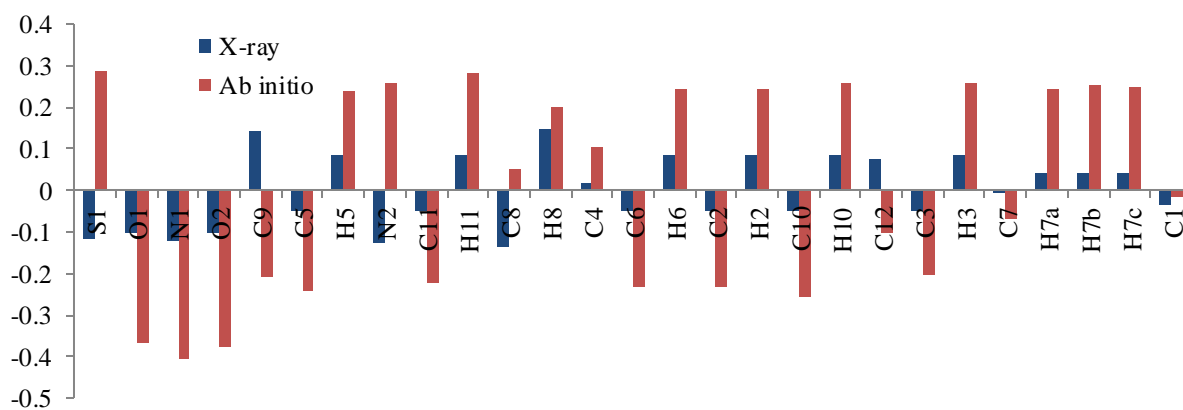


Fig. 5. Atomic charges of the title molecule

### 3.4. HOMO and LUMO energies

The highest occupied molecular orbitals (HOMOs) and lowest-lying unoccupied molecular orbitals (LUMO) are very useful for physicists and chemists because the energy difference between these orbitals (energy gap) represents the minimum energy required to promote an electron, and is therefore often the most-frequent and important energy transfer mechanism within a system. The orbitals also provide important electron density information which can help determine which part of the

Table 6. Atomic charges of  $C_{12}H_{10}N_2O_2S$  molecule

Atoms	$q_{x\text{-ray}}$	$q_{ab\text{ initio}}$
S1	-0.115	0.487
O1	-0.102	-0.367
N1	-0.123	-0.407
O2	-0.102	-0.377
C9	0.144	-0.207
C5	-0.049	-0.242
H5	0.085	0.240
N2	-0.125	0.459
C11	-0.049	-0.224
H11	0.085	0.282
C8	-0.135	0.053
H8	0.146	0.202
C4	0.018	0.103
C6	-0.049	-0.231
H6	0.085	0.242
C2	-0.049	-0.233
H2	0.085	0.243
C10	-0.049	-0.256
H10	0.085	0.261
C12	0.078	-0.104
C3	-0.049	-0.204
H3	0.085	0.257
C7	-0.007	-0.709
H7A	0.044	0.245
H7B	0.044	0.254
H7C	0.044	0.250
C1	-0.036	-0.015

molecule is most actively participating in an energy transfer event. The HOMO-LUMO energy gap of the molecule was calculated using B3LYP/6-31G(d,p) level as presented in Table 7. The energy gap between HOMO and LUMO indicates molecular chemical stability. In addition, a lower HOMO-LUMO energy gap (3.22 eV) calculated at B3LYP/6-31G(d,p) explains the fact that eventual charge transfer interaction is taking place within the molecule. The HOMO-LUMO plots are given in Fig. 6.

Table 7. HOMO-LUMO energies of the molecule

Energies	HF/6-31G(d,p)	DFT/6-31G(d,p)
$E_{\text{HOMO}}$	-0.30855	-0.22761
$E_{\text{LUMO}}$	0.02852	-0.10917
$E_{\text{Gap}}$ (a.u.)	0.33707	0.11844
$E_{\text{Gap}}$ (eV)	9.17	3.22

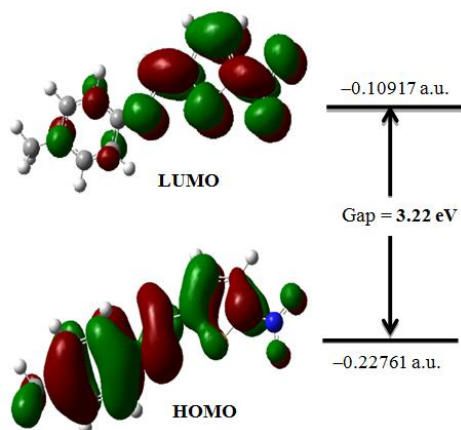


Fig. 6. The HOMO and LUMO plot of the title molecule at B3LYP/6-31G(d,p)

### 3.5. Molecular electrostatic potential

The electrostatic potential  $V(\vec{r})$ , at a given point  $\vec{r}(x, y, z)$  in the space around a molecule (in atomic units) is defined in terms of the interaction energy between the electrical charge generated from the molecule electrons and nuclei and positive test charge (a proton) located at  $\vec{r}$  and can be expressed as:

$$V(\vec{r}) = \sum_A \frac{Z_A}{|\vec{R}_A - \vec{r}|} - \int \frac{\rho(\vec{r}') d\vec{r}'}{|\vec{r}' - \vec{r}|}$$

where  $Z_A$  is the charge on nucleus A, located at  $\vec{R}_A$  and  $\rho(\vec{r}')$  is the electronic density function for the molecule. The first and second terms represent the contributions to the potential due to nuclei and electrons, respectively.  $V(\vec{r})$  is the resultant electrical potential at each point  $\vec{r}$ , which is the net electrostatic effect produced at the point  $\vec{r}$  by both the electrons and nuclei of the molecule. The molecular electrostatic potential (MEP) serves as a useful quantity to explain hydrogen bonding, reactivity and structure-activity relationship of the molecules [36].

In order to predict the molecular reactive sites, the MEP for the title molecule was calculated using 6-31G(d,p) basis set and shown together with the experimental one in Fig. 7. The different values of the electrostatic potential at the surface are represented by different colors, where blue indicates the highest electrostatic potential energy and red indicates the lowest electrostatic potential energy. As it can be seen from the MEP map of the title compound, the region around oxygen atoms linked with carbon through double bond represents the most negative potential region (red). The most negative  $V(\vec{r})$  value is

associated also with  $\text{NO}_2$  group. The hydrogen atoms attached to nitrogen atoms possess the maximum positive charge. The MEP surface provides necessary details about the reactive sites.

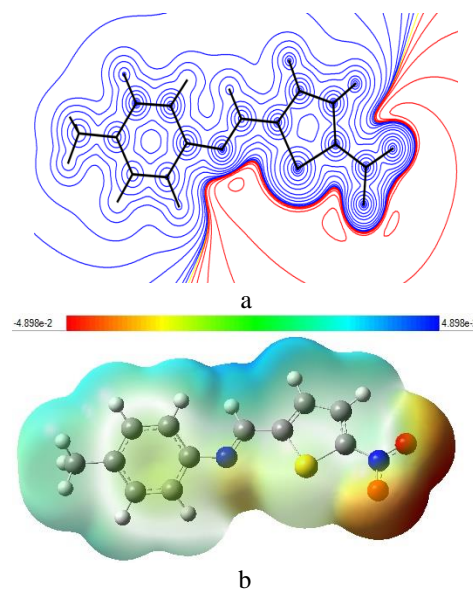


Fig. 7. Molecular electrostatic potential maps (a) experimental (b) calculated at B3LYP/6-31G(d,p) level

### 3.6. Nonlinear optical (NLO) properties

For organic NLO materials, theoretical and experimental studies are performed in order to understand the microscopic origin of nonlinear behavior [37, 38].

In this context, this study is extended to the determination of the electric dipole moment  $\mu$ , the isotropic polarizability  $\alpha$  and the first hyperpolarizability  $\beta_{tot}$  of the title compound.

The dipole moment ( $\mu$ ), isotropic polarizability ( $\alpha$ ), first-order hyperpolarizability ( $\beta_{tot}$ ) tensor, can be obtained using the following equations:

$$\mu_0 = (\mu_x^2 + \mu_y^2 + \mu_z^2)^{1/2}$$

$$\alpha = \frac{1}{3} (\alpha_{xx} + \alpha_{yy} + \alpha_{zz})$$

$$\beta_{tot} = (\beta_x^2 + \beta_y^2 + \beta_z^2)^{1/2}$$

The whole equation for computing the magnitude of the first hyperpolarizability ( $\beta$ ) from Gaussian 03 output is given below:

$$\beta_{tot} = \left[ (\beta_{xxx} + \beta_{xyy} + \beta_{xzz})^2 + (\beta_{yyy} + \beta_{yzz} + \beta_{yxx})^2 + (\beta_{zzz} + \beta_{zxx} + \beta_{zyy})^2 \right]^{1/2}$$

The first hyperpolarizability is a third rank tensor that can be depicted by a  $3 \times 3 \times 3$  matrices. The 27 components of the 3D matrix can be reduced to 10 components because of the Kleinman symmetry [39]. The Gaussian 03 output provides 10 components of this matrix

as  $\beta_{xxx}$ ,  $\beta_{xyx}$ ,  $\beta_{xyy}$ ,  $\beta_{yyy}$ ,  $\beta_{xxz}$ ,  $\beta_{xyz}$ ,  $\beta_{yyz}$ ,  $\beta_{xzz}$ ,  $\beta_{yzz}$ ,  $\beta_{zzz}$  respectively.

The first hyperpolarizability tensors provided by Gaussian 03 are given in atomic units (a.u.), the computed values were converted into electrostatic units. ( $\alpha$ : 1 a.u. =  $0.1482 \times 10^{-24}$  esu ;  $\beta$ : 1 a.u. =  $8.6393 \times 10^{-33}$  esu).

The dipole moment ( $\mu_0$ ), mean polarizability ( $\alpha$ ) and first hyperpolarizability ( $\beta$ ) are calculated at 6-31G(d,p) basis set. Table 8 and 9 give the HF and B3LYP results of the electronic dipole moment  $\mu_i$  ( $i = x, y, z$ ), polarizability  $\alpha_{ij}$  and the first hyperpolarizability  $\beta_{ijk}$  for 4-methyl-N-[(5-nitrothiophen -2-yl)methylidene)] aniline compound. Theoretical calculation plays a significant role in understanding the structure-property relationship which is able to help in designing novel NLO materials. It is well established that the higher values of dipole moment, molecular polarizability, and hyperpolarizability are very important for active NLO properties. The highest value of

dipole moment obtained from multipolar refinement is equal to 7.10 D. The highest value of dipole moment is observed for component  $\mu_x$ . In this direction, this value is equal to 5.5421. Figure 8 shows the orientation of the molecular dipole moment of the title molecule. The calculated polarizability ( $\alpha$ ), is about to  $2.5 \times 10^{-23}$  esu obtained with 6-31G(d,p) basis set. As it can be seen in Table 9, the calculated polarizability  $\alpha_{ij}$  have non zero values and was dominated by the diagonal components. The first hyperpolarizability value  $\beta_{tot}$  of the title molecule obtained with B3LYP/6-31G(d,p) is  $26.77 \times 10^{-30}$  esu. The calculated results show that the title molecule might have microscopic nonlinear (NLO) behavior with non-zero values.

The calculated first order hyperpolarizability of the title molecule is found to be 137 times greater than the  $\beta_{total}$  value of urea ( $0.1947 \times 10^{-30}$  esu), therefore, predicting that our molecule is a powerful candidate for NLO material.

Table 8. The molecular dipole moment of the  $C_{12}H_{10}N_2O_2S$  obtained by X-ray, HF and DFT/B3LYP methods.

Methods	Models	$\mu_x$ (e.Å)	$\mu_y$ (e.Å)	$\mu_z$ (e.Å)	$\ \vec{\mu}\ $ (D)
X-Ray	Multipole refinement	3.8105	4.5369	-3.4954	7.10
Ab initio	B3LYP/6-31G(d,p)	5.5421	3.7709	-0.6531	6.74
	HF/6-31G(d,p)	-5.3130	4.3369	-1.0518	6.94

From the cited above results, the molecule having the greatest  $\beta_{tot}$  value, corresponds to the low HOMO-LUMO energy gap. These results show that HOMO-LUMO gap have a substantial influence on the first hyperpolarizability. The high  $\beta$  value and low HOMO-LUMO energy gap show that the title molecule is highly NLO active material and it might be efficient for optoelectronic applications.

Consequently, we can finally infer from the above discussion that the introduction of electron correlation in the method applied for the analysis of the hyperpolarizability, such as DFT method, will probably predict more reasonable values as opposed to those converged upon use of the HF method.

Table 9. Polarizability ( $\alpha$ ) and hyperpolarizability ( $\beta$ ) values of the  $C_{12}H_{10}N_2O_2S$  molecule obtained by HF and DFT/B3LYP using 6-31G(d,p) basis set.

Parameters	6-31G(d,p)		Parameters	6-31G(d,p)	
	HF	DFT		HF	DFT
$\alpha_{xx}$	207.764	303.976	$\beta_{xxx}$	3039.846	3144.213
$\alpha_{xy}$	16.225	18.334	$\beta_{xyx}$	-119.167	-235.328
$\alpha_{yy}$	103.406	157.183	$\beta_{xyy}$	-4.692	-32.563
$\alpha_{xz}$	-3.316	-3.689	$\beta_{yyy}$	20.662	80.005
$\alpha_{yz}$	2.975	2.861	$\beta_{xxz}$	-17.024	-14.027
$\alpha_{zz}$	27.538	65.453	$\beta_{xyz}$	-13.185	-32.687
$\alpha$ (a.u.)	112.902	175.537	$\beta_{yyz}$	-3.226	-13.999
$\alpha \times 10^{-23}$ (esu)	<b>2.48</b>	<b>2.60</b>	$\beta_{xzz}$	2.348	-21.954
			$\beta_{yzz}$	5.097	-7.938
			$\beta_{zzz}$	-5.577	-10.061
			$\beta$ (a.u.)	3039.047	3098.873
			$\beta \times 10^{-30}$ (esu)	<b>26.26</b>	<b>26.77</b>

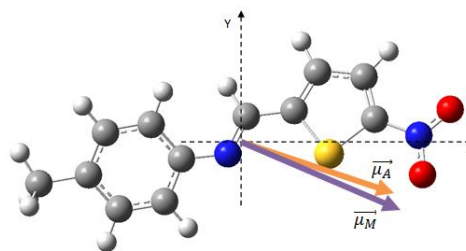


Fig. 8. Orientation of the molecular dipole moment of  $C_{12}H_{10}N_2O_2S$  molecule  
 $\vec{\mu}_M$ : Experimental molecular dipole moment,  $\vec{\mu}_A$ : Calculated molecular dipole moment

#### 4. Conclusion

In the present work, we have performed theoretical calculation on 4-methyl-N-[(5-nitrothiophen-2-ylmethylidene)] aniline molecule which leads to an optimized structure with bond lengths and bond angles closer to the X-ray experiment results. On the other hand, high resolution X-ray experiment crystallographic data were used to investigate the electron charge density of the title compound. We have also shown that electron density can yield to electronic experimental proprieties such as atomic charges, dipole moment and electrostatic potential. Using theoretical structural results, we have calculated atomic charges, HOMO–LUMO energy, molecular electrostatic potential, and nonlinear optical properties for the organic molecule 4-methyl-N-[(5-nitrothiophen-2-ylmethylidene)] aniline. Molecular properties have been calculated by using ab initio HF and DFT (B3LYP) methods with 6-31G(d,p) basis set. The molecular electrostatic potential map shows that the negative potential sites are on the electronegative atoms as well as the positive potential sites are around the hydrogen atoms. These sites give information about the possible regions for inter- and intramolecular hydrogen bonding. The calculated dipole moment mean value of the studied compound is 7.10 D obtained using multipolar refinement which is in agreement with the value (about 7.0 D) calculated by theoretical methods. The mean polarizability ( $\alpha$ ) and the total first static hyperpolarizability ( $\beta_{total}$ ) of the molecule are found to be  $2.5 \times 10^{-23}$  esu and  $26.77 \times 10^{-30}$  esu, respectively. The computed  $\beta_{total}$  value is nearly 137 times more than  $\beta_{total}$  of urea, inferring that our molecule to be a potential candidate for nonlinear optical applications. HOMO-LUMO energy gap explains the eventual charge transfer interactions taking place within the molecule. Furthermore, the first-order hyperpolarizability and total dipole moment property of the molecule show that the title molecule is an attractive target for future studies of nonlinear optical properties.

#### References

- [1] J. Zyss, I. Ledoux, M. Bertault, E. Toupet, *Chemical Physics* **150**, 125 (1991).
- [2] I. Ledoux, J. Zyss, *Molecular Nonlinear Optics: Fundamentals and Applications*, (I.C. Khoo, F. Simoni, C. Umeton, Ed.) pp. 1, 1997.
- [3] D.S. Chemla, J. Zyss, *Nonlinear Optical Properties of Organic Molecules and Crystals*, Academic Press, New York 1987.
- [4] H. Qin, S. Wenger, M. Xu, F. Gao, X. Jing, P. Wang, S. M. Zakeeruddin, M. Grätzel, *J. Am. Chem. Soc.* **130**, 9202 (2008).
- [5] H. Ünver, A. Karakas, A. Elmali, *J. Mol. Struct.* **702**, 49 (2004).
- [6] H. Tanak, A. A. Ağar, O. Büyükgüngör, *Spectrochim. Acta Part A* **87**, 15 (2012).
- [7] H. Tanak, A. A. Ağar, O. Büyükgüngör, *Spectrochimica Acta Part A* **118**, 672 (2014).
- [8] H. Tanak, A.A. Ağar, O. Büyükgüngör, *J. Mol. Struct.* **1048**, 41 (2013).
- [9] R. M. F. Batista, S.P.G. Costa, M. Belsley, M. M. M. Raposo, *Dyes Pigm.* **80**, 329 (2009).
- [10] L. Xiao-Hong, Z. Xian-Zhou, *Spectrochim. Acta Part A* **105**, 280 (2013).
- [11] Y. Megrouss, N. Benhalima, R. Bahoussi, N. Boukabcha, A. Chouaih, F. Hamzaoui, *Chin. Phys. B* **24**(10), 106103 (2015).
- [12] F. Hamzaoui, F. Baert, J. Zyss, *J. Mater. Chem.* **6**, 1123 (1996).
- [13] F. Hamzaoui, A. Zanoun, G. Vergoten, *J. Mol. Struct.* **697**(1–3), 17 (2004).
- [14] A. Chouaih, F. Hamzaoui, G. Vergoten, *J. Mol. Struct.* **738**(1–3), 33 (2005).
- [15] N. Benhalima, K. Toubal, A. Chouaih, G. Chita, S. Maggi, A. Djafri, F. Hamzaoui, *J. Chem. Crystallogr.* **41**(11), 1729 (2011).
- [16] M. Drissi, A. Chouaih, Y. Megrouss, F. Hamzaoui, *Journal of Crystallography* **2013**, ID 326457 (2013).
- [17] N. Boubegra, A. Chouaih, M. Drissi, F. Hamzaoui, *Chin. Phys. B* **23**(1), 016103 (2014).
- [18] C. Jelsch, B. Guillot, A. Lagoutte, C. Lecomte, *J. Appl. Crystallogr.* **38**, 1 (2005).
- [19] M. J. Frisch, G. W. Trucks, H. B. Schlegel, G. E. Scuseria, M. A. Robb, J. R. Cheeseman, J. A. Montgomery, T. Vreven, K. N. Kudin, J. C. Burant, J. M. Millam, S. S. Iyengar, J. Tomasi, V. Barone, B. Mennucci, M. Cossi, G. Scalmani, N. Rega, G. A. Petersson, H. Nakatsuji, M. Hada, M. Ehara, K. Toyota, R. Fukuda, J. Hasegawa, M. Ishida, T. Nakajima, Y. Honda, O. Kitao, H. Nakai, M. Klene, X. Li, J. E. Knox, H. P. Hratchian, J. B. Cross, V. Bakken, C. Adamo, J. Jaramillo, R. Gomperts, R. E. Stratmann, O. Yazyev, A. J. Austin, R. Cammi, C. Pomelli, J. W. Ochterski, P. Y. Ayala, K. Morokuma, G. A. Voth, P. Salvador, J. J. Dannenberg, V. G. Zakrzewski, S. Dapprich, A. D. Daniels, M. C. Strain, O. Farkas, D. K. Malick, A. D. Rabuck, K. Raghavachari, J. B. Foresman, J. V. Ortiz, Q. Cui, A. G. Baboul, S. Clifford, J. Cioslowski, B. B. Stefanov, G. Liu, A. Liashenko, P. Piskorz, I. Komaromi, R. L. Martin, D. J. Fox, T. Keith, M. A. Al-Laham, C.Y. Peng, A. Nanayakkara, M. Challacombe, P.M. W. Gill, B. Johnson, W. Chen, M.W. Wong, C. Gonzalez, J.A. Pople, Gaussian 03, Revision C.02, Gaussian, Inc., Wallingford CT, USA, 2004.
- [20] M. Cai, X. Wang, T. Sun, *Acta Cryst. E* **67**, o2218 (2011).
- [21] T. Akbal, E. Agar, S. Gümüş, A. Erdönmez, *Acta Cryst. E* **68**, o3026 (2012).
- [22] T. Akbal, E. Agar, S. Gümüş, A. Erdönmez, *Acta Cryst. E* **68**, o2673 (2012).
- [23] N. Kan Kaynar, S. Gümüş, E. Agar, O. Büyükgüngör, M. Yavuz, *Acta Cryst. E* **68**, o393 (2012).

- [24] Ü. Ceylan, S. Gümüs, E. Agar, M.S. Soylu, *Acta Cryst. E* **68**, o2116 (2012).
- [25] Ü. Ceylan, H. Tanak, S. Gümüs, E. Agar, *Acta Cryst. E* **67**, o2004 (2011).
- [26] N.K. Hansen, P. Coppens, *Acta Cryst. A* **34**, 909 (1978).
- [27] A. E. Frisch, A. B. Nielsen, A. J. Holder, *Gaussview*. Gaussian Inc., Pittsburg, PA 2003.
- [28] A. D. Becke, *J. Chem. Phys.* **107**, 8554 (1997).
- [29] G. Rauhut, P. Pulay, *J. Phys. Chem.* **99**, 3093 (1995).
- [30] H.D. Cohen, C.C. Roothaan, *J. Chem. Phys.* **43**, S34 (1965).
- [31] R. Fletcher, M.J.D. Powell, *Comput. J.* **6**, 163 (1963).
- [32] R.F. Bader, *Atoms in molecules. A quantum theory*. Clarendon Press, Oxford 1990.
- [33] P. Coppens, *X-Ray Charge Densities and Chemical Bonding*, Oxford, New York 1997.
- [34] M.A. Spackman, "Charge densities from X-ray diffraction data," *Annual Reports on the Progress of Chemistry C* **94**, 177 (1998).
- [35] R.H. Blessing, *J. Appl. Cryst.* **22**, 396 (1989).
- [36] S. Chidangil, M. K. Shukla, P. C. Mishra, *J. Mol. Model.* **4**, 250 (1998).
- [37] P. Kerkoc, M. Zgonik, K. Sutter, C. Bosshard, P. Gunter, *J. Opt. Soc. Am. B* **7**, 313 (1990)
- [38] D. Sajan, H.J. Ravindra, M. Neeraj, I. Hubert Joe, *Vibrational Spectroscopy* **54**, 72 (2010).
- [39] D. A. Kleinman, *Phys. Rev.* **126**, 1977 (1962).

---

\*Corresponding author: achouaih@gmail.com